



# Forced convection of turbulent flow into the wavy parallel channel

Ammar I. Alsabery<sup>1,2</sup> · Mikhail A. Sheremet<sup>3</sup> · Ali J. Chamkha<sup>4</sup> · Ishak Hashim<sup>2</sup>

Received: 19 October 2021 / Accepted: 20 March 2022 / Published online: 15 April 2022  
© Akadémiai Kiadó, Budapest, Hungary 2022

## Abstract

The energy transport enhancement is a topical problem for many engineering applications. One of the possible solutions to this problem is an improvement of the heat transfer surface. The present investigation is devoted to numerical simulation regarding turbulent forced convective energy transport inside a curved channel under the isothermal heating from the upper wavy wall and cooling from the inlet section. The governing partial differential equations written using the Reynolds-averaged Navier-Stokes formulation including the standard  $k - \epsilon$  approach have been solved numerically by the finite-element procedure. Impacts of the Reynolds number, undulations number and undulations amplitude toward fluid motion and energy transport have been scrutinized. With the undulations number, a significant energy carrier condensation has been detected.

**Keywords** Forced convection · Heat transfer · Turbulent flow · Wavy walls · Horizontal channel

## Introduction

Forced and mixed convection is the primary energy transport phenomena in many industrial systems where engineers employ open-ended channels. Such open-ended channels can be used for cooling of heated surfaces [1–5], and the energy transport enhancement can be accomplished by the inclusion of the extended heat transfer surface [6, 7]. Presently there are many published articles toward the numerical and experimental analysis of energy transport and flow structures within corrugated channels [7–10]. Thus, Miroshnichenko et al. [8] used numerical simulation to investigate the mixed convection of micropolar fluid into a horizontal wavy channel including the influence of local isothermal heater at the wavy bottom surface. Impacts of the eddy

viscosity parameter and Prandtl number have been studied, where authors have shown that a rise of Pr characterizes the energy transport intensification. Vo et al. [9] have investigated computationally  $\gamma$ -AlOOH nanofluid motion through a wavy channel under the heating effect from wavy part of the channel. Authors have shown that a rise of the amplitude of the wavy component illustrates the growth of the performance evaluation criteria index firstly. Still, after achieving the maximum value, this parameter decreases. Numerical analysis of copper-water nanofluid mixed convection connected by entropy production inside the horizontal channel with the wavy part has been achieved by Dormohammadi et al. [10]. Employing Fluent software, contributors have examined the influence from the Richardson number, undulations amplitude, wavelength ratio and nanoparticles volume fraction on flow structures and temperature patterns. It has been revealed that a sinusoidal wavy wall can enhance energy transport.

It should be noted that application of mono and hybrid nanofluids is very useful and important for different thermal systems [11–16]. Thus, Jamshidmofid and Bahiraei [11] studied numerically the influence of three types of nanofluids on heat transfer performance in two kinds of wavy microchannels using multi-phase mixture approach. It has been found that an essential intensification of convective heat transfer is for the up-down wavy microchannel filled with silver/water nanofluid. Alrowaili et al. [12] investigated natural convection combined with thermal radiation

✉ Ishak Hashim  
ishak\_h@ukm.edu.my

<sup>1</sup> Refrigeration & Air-conditioning Technical Engineering Department, College of Technical Engineering, The Islamic University, Najaf, Iraq

<sup>2</sup> Department of Mathematical Sciences, Faculty of Science & Technology, Universiti Kebangsaan Malaysia, UKM, 43600 Bangi, Selangor, Malaysia

<sup>3</sup> Department of Theoretical Mechanics, Tomsk State University, Tomsk, Russia 634050

<sup>4</sup> Faculty of Engineering, Kuwait College of Science and Technology, Doha District 35004, Kuwait

of the power-law nanofluids in wavy chamber. The authors have shown that the shape of wavy walls have an essential influence on heat transfer performance. Kumar et al. [13] have analyzed alumina/water nanofluid cooling behavior in a branched wavy heat sink microchannel. Using RNG  $k - \epsilon$  turbulence model, the authors have revealed that branched wavy microchannel illustrates a formation of the secondary flow enhancing the macroscopic mixing. Jahanbakhshi et al. [14] have scrutinized numerically nanofluid flow and heat transfer to cool the lithium-ion battery with a presence of wavy microchannels and microtubes. Using ANSYS FLU-ENT software the authors have ascertained that using the heat sink diminishes the battery surface temperature, while an addition of nanoparticles allows to keep the temperature within a safe working range. Numerical simulation of hybrid nanofluid flow and energy transport in a parabolic trough solar collector receiver's tube equipped with wavy promoters has been performed by Mohammed et al. [15]. It has been shown that using the wavy promoters within the tube can essentially enhance the heat performance. Computational analysis of MHD power-law hybrid nanoliquid flow and heat transfer within a wavy micro-tube having porous disks has been performed by Derikvand and Rahmati [16]. The authors have shown that a rise of the nanoparticles volume fraction allows intensifying the heat transfer.

Perng and Wu [17] numerically investigated thermal parameters in 3D gas wavy channels under the methanol steam reformation. Authors have shown that undulations allow intensifying the transport processes. The mixing of two various gases within the wavy channel has been examined numerically by Borgohain et al. [18] using the in-house computational code. The obtained results have shown that for high amplitude, the mixing process will be better, and for low Reynolds number, the mixing process can be improved using the wavy walls. Nguyen et al. [19] have scrutinized computationally nanofluid forced convection in a wavy channel within inner obstacles. Authors have demonstrated the energy transport strengthening with a rise of the wavelength. Numerical and experimental analysis regarding forced convection cooling of the wavy heat sink, including rectangular ribs under the influence of alumina/water nanofluid has been performed by Khoshvaght-Aliabadi et al. [20]. The obtained outcomes have revealed that the ribbed wavy heat sink improves the energy transfer, while the growth of the alumina concentration raises heat transfer strength. Yuan et al. [21] numerically and experimentally have examined the rough microchannels' influence on the transport processes intensification. It has been ascertained that the divergent wavy microchannel has an optimal value of the flow resistance and heat transfer rate. Job and Gunakala [22] have numerically analysed MHD mixed convection of water-based nanoliquids into a horizontal corrugated channel with two heated solid cylinders. They have presented

that the used channel with grooved walls can strengthen the energy transport within the channel. An influence of porous insertions on energy removal from the heated element within the wavy nanofluid channel has been investigated numerically by Job and Gunakala [23]. Authors have shown that the temperature close to the heated elements can be diminished by rising the Grashof, Reynolds and Eckert numbers. Other interesting results on laminar mixed convection can be found in [24–26].

Taking into account this performed brief review, it is possible to conclude that fluid flow in corrugated channels have many applications in practice including the optimization of heat exchangers and solar collectors, cooling of electronic devices and heat-generating elements and others. It is well-known that using the channel or tube geometry the flow regime for intensive fluid motion is turbulent. Therefore, detailed analysis of turbulent flow and heat transfer is very useful for optimization of different thermal systems mentioned above. At the same time, the heat transfer rate increases when the turbulent flows are developed. In the case of turbulent flows within the corrugated channels, the obtained results [27–33] are not as comprehensive as the laminar regime. Therefore, the present research deals with numerical simulation regarding turbulent forced convection within a wavy channel under the upper wall heating. Such formulation allows studying an impact of upper isothermal wavy wall on turbulent flow and formation of mixing zones within wavy channel that is useful for heat transfer enhancement. Thermal and flow features of turbulent fluid flow in a wavy channel under heating of the upper wavy wall have not been investigated previously taking into account the published papers. Moreover, detailed analysis performed in the present research illustrating an influence of Reynolds number, undulations number and amplitude shows and opportunity to enhance the convective heat transfer within wavy channels.

## Mathematical formulation

Inside a 2D wavy channel with length  $L$  and height  $h$ , we investigate steady forced convection flow and heat transfer problems which is reported by Fig. 1. The heat source is at a fixed temperature ( $T_h$ ) upon on upper wavy surface, while the lower surface is presumed to be adiabatic.

The inlet fluid flow including cold temperature ( $T_c$ ) includes approaching the wavy channel of the left section with consistent horizontal velocity ( $u_{in}$ ) left vertical surface. In contrast, the fluid outlet field remains flowing of the right adiabatic section of the channel among fixed pressure ( $p = 0$ ). The space between the wavy surfaces is filled with water. The Boussinesq approximation remains relevant. Concerning the assumptions as stated briefly, the

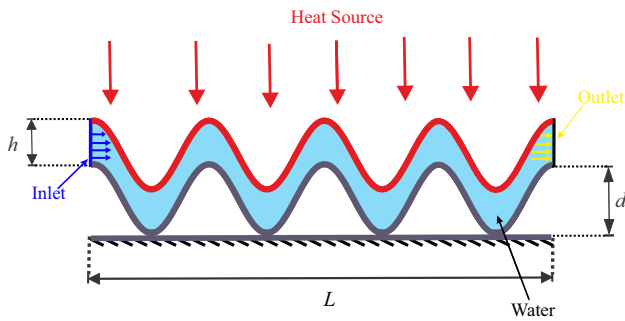


Fig. 1 Schematic diagram of the wavy channel.

Navier-Stokes and energy equations of the incompressible Newtonian fluid with the turbulent flow can be formulated as the following:

$$\frac{\partial u}{\partial x} + \frac{\partial v}{\partial y} = 0, \tag{1}$$

$$\begin{aligned} \frac{\partial}{\partial x}(uu) + \frac{\partial}{\partial y}(uv) &= -\frac{1}{\rho_f} \frac{\partial p}{\partial x} + 2 \frac{\partial}{\partial x} \left( v_{\text{eff}} \frac{\partial u}{\partial x} \right) \\ &+ \frac{\partial}{\partial y} \left( v_{\text{eff}} \frac{\partial u}{\partial y} \right) \\ &+ \frac{\partial}{\partial y} \left( v_{\text{eff}} \frac{\partial v}{\partial x} \right), \end{aligned} \tag{2}$$

$$\begin{aligned} \frac{\partial}{\partial x}(uv) + \frac{\partial}{\partial y}(vv) &= -\frac{1}{\rho_f} \frac{\partial p}{\partial y} + \frac{\partial}{\partial x} \left( v_{\text{eff}} \frac{\partial v}{\partial x} \right) \\ &+ \frac{\partial}{\partial x} \left( v_{\text{eff}} \frac{\partial u}{\partial y} \right) \\ &+ 2 \frac{\partial}{\partial y} \left( v_{\text{eff}} \frac{\partial v}{\partial y} \right), \end{aligned} \tag{3}$$

$$\begin{aligned} \frac{\partial}{\partial x}(uT) + \frac{\partial}{\partial y}(vT) &= \frac{\partial}{\partial x} \left[ \left( \frac{k_f}{\rho_f C_{pf}} + \frac{v_f}{Pr_t} \right) \frac{\partial T}{\partial x} \right] \\ &+ \frac{\partial}{\partial y} \left[ \left( \frac{k_f}{\rho_f C_{pf}} + \frac{v_f}{Pr_t} \right) \frac{\partial T}{\partial y} \right] \end{aligned} \tag{4}$$

The turbulent kinetic energy ( $k$ ) and dissipation rate ( $\epsilon$ ) are:

$$\begin{aligned} \frac{\partial}{\partial x}(uk) + \frac{\partial}{\partial y}(vk) &= \frac{\partial}{\partial x} \left[ \left( v_f + \frac{v_t}{\sigma_k} \right) \frac{\partial k}{\partial x} \right] + \frac{\partial}{\partial y} \left[ \left( v_f + \frac{v_t}{\sigma_k} \right) \frac{\partial k}{\partial y} \right] + P_k - \epsilon, \end{aligned} \tag{5}$$

$$\begin{aligned} \frac{\partial}{\partial x}(u\epsilon) + \frac{\partial}{\partial y}(v\epsilon) &= \frac{\partial}{\partial x} \left[ \left( v_f + \frac{v_t}{\sigma_\epsilon} \right) \frac{\partial \epsilon}{\partial x} \right] + \frac{\partial}{\partial y} \left[ \left( v_f + \frac{v_t}{\sigma_\epsilon} \right) \frac{\partial \epsilon}{\partial y} \right] \\ &+ (C_{1\epsilon} P_k - C_{2\epsilon} \epsilon) \frac{\epsilon}{k}, \end{aligned} \tag{6}$$

where  $v_{\text{eff}} = v_f + v_t$ ,  $P_k = v_t \left[ 2 \left( \frac{\partial u}{\partial x} \right)^2 + 2 \left( \frac{\partial v}{\partial y} \right)^2 + \left( \frac{\partial u}{\partial y} + \frac{\partial v}{\partial x} \right)^2 \right]$  and  $v_t = C_\mu \frac{k^2}{\epsilon}$ .

The following non-dimensional variables are now incorporated:

$$\begin{aligned} X = \frac{x}{L}, \quad Y = \frac{y}{L}, \quad U, V = \frac{u, v}{U_i}, \quad P = \frac{P}{\rho_f U_i^2}, \\ k_n = \frac{k}{U_i^2}, \quad \epsilon_n = \frac{\epsilon L}{U_i^3}. \end{aligned} \tag{7}$$

Here then generates the dimensionless governing equations as:

$$\frac{\partial U}{\partial X} + \frac{\partial V}{\partial Y} = 0, \tag{8}$$

$$\begin{aligned} U \frac{\partial U}{\partial X} + V \frac{\partial U}{\partial Y} &= -\frac{\partial P}{\partial X} + 2 \frac{\partial}{\partial X} \left[ \left( \frac{1}{Re} + \bar{v}_t \right) \frac{\partial U}{\partial X} \right] \\ &+ \frac{\partial}{\partial Y} \left[ \left( \frac{1}{Re} + \bar{v}_t \right) \frac{\partial U}{\partial Y} \right] + \frac{\partial}{\partial Y} \left[ \left( \frac{1}{Re} + \bar{v}_t \right) \frac{\partial V}{\partial X} \right], \end{aligned} \tag{9}$$

$$\begin{aligned} U \frac{\partial V}{\partial X} + V \frac{\partial V}{\partial Y} &= -\frac{\partial P}{\partial Y} + \frac{\partial}{\partial X} \left[ \left( \frac{1}{Re} + \bar{v}_t \right) \frac{\partial V}{\partial X} \right] \\ &+ \frac{\partial}{\partial X} \left[ \left( \frac{1}{Re} + \bar{v}_t \right) \frac{\partial U}{\partial Y} \right] + 2 \frac{\partial}{\partial Y} \left[ \left( \frac{1}{Re} + \bar{v}_t \right) \frac{\partial V}{\partial Y} \right], \end{aligned} \tag{10}$$

$$\begin{aligned} U \frac{\partial \theta}{\partial X} + V \frac{\partial \theta}{\partial Y} &= \frac{\partial}{\partial X} \left[ \left( \frac{1}{Re Pr} + \frac{\bar{v}_t}{Pr_t} \right) \frac{\partial \theta}{\partial X} \right] \\ &+ \frac{\partial}{\partial Y} \left[ \left( \frac{1}{Re Pr} + \frac{\bar{v}_t}{Pr_t} \right) \frac{\partial \theta}{\partial Y} \right], \end{aligned} \tag{11}$$

The dimensionless turbulent kinetic energy ( $k_n$ ) and dimensionless turbulent dissipation rate ( $\epsilon_n$ ) are:

$$\begin{aligned} U \frac{\partial k_n}{\partial X} + V \frac{\partial k_n}{\partial Y} &= \frac{\partial}{\partial X} \left[ \left( \frac{1}{Re} + \frac{\bar{v}_t}{\sigma_k} \right) \frac{\partial k_n}{\partial X} \right] \\ &+ \frac{\partial}{\partial Y} \left[ \left( \frac{1}{Re} + \frac{\bar{v}_t}{\sigma_k} \right) \frac{\partial k_n}{\partial Y} \right] \\ &+ \bar{P}_k - \epsilon_n, \end{aligned} \tag{12}$$

$$\begin{aligned} U \frac{\partial \epsilon_n}{\partial X} + V \frac{\partial \epsilon_n}{\partial Y} &= \frac{\partial}{\partial X} \left[ \left( \frac{1}{Re} + \frac{\bar{v}_t}{\sigma_\epsilon} \right) \frac{\partial \epsilon_n}{\partial X} \right] + \frac{\partial}{\partial Y} \\ &\left[ \left( \frac{1}{Re} + \frac{\bar{v}_t}{\sigma_\epsilon} \right) \frac{\partial \epsilon_n}{\partial Y} \right] + C_{1\epsilon} \bar{P}_k \frac{\epsilon_n}{k_n} - C_{2\epsilon} \frac{\epsilon_n^2}{k_n}, \end{aligned} \tag{13}$$

where  $Re = \frac{U_i L}{\nu_r}$  is the Reynolds number,  $Pr = \frac{\nu_r}{\alpha_r}$  is the Prandtl number,  $\bar{P}_k = \bar{\nu}_t \left[ 2 \left( \frac{\partial U}{\partial X} \right)^2 + 2 \left( \frac{\partial V}{\partial Y} \right)^2 + \left( \frac{\partial U}{\partial Y} + \frac{\partial V}{\partial X} \right)^2 \right]$  and  $\bar{\nu}_t = C_\mu \frac{k_n^2}{\epsilon_n}$  is the dimensionless turbulent viscosity.

The selected boundary conditions are:

At the top of the hot wavy surface:

$$u = 0, v = 0, T = T_h, 0 \leq x \leq L, \quad (14)$$

$$d - A(1 - \cos(N\pi y)),$$

At left surface with the cold inlet flow:

$$u = u_{in}, v = 0, T = T_c, k = \frac{3}{2}(u_{in} I)^2, \quad (15)$$

$$\epsilon = C_\mu^{\frac{3}{4}} \frac{k^{\frac{3}{2}}}{L}, x = 0, 0 \leq y \leq 1,$$

At the lower adiabatic wavy surface:

$$u = 0, v = 0, \frac{\partial T}{\partial n} = 0, 0 \leq x \leq L, \quad (16)$$

$$h - A(1 - \cos(N\pi y)),$$

where  $n$  is the direction normal to the wavy surface.

At the right adiabatic outlet surface:

$$u = v = 0, p = 0, \frac{\partial T}{\partial x} = 0, \frac{\partial k}{\partial x} = 0, \quad (17)$$

$$\frac{\partial \epsilon}{\partial x} = 0, x = 1, 0 \leq y \leq 1,$$

The local Nusselt number is calculated along the heated upper wavy surface as the following:

$$Nu = -\sqrt{\left( \frac{\partial \theta}{\partial X} \right)^2 + \left( \frac{\partial \theta}{\partial Y} \right)^2}. \quad (18)$$

and the average Nusselt number ( $\bar{Nu}$ ) is determined by the integration of the local Nusselt number along the upper wavy surface, which remains defined by:

$$\bar{Nu} = \frac{1}{S} \int_0^S Nu dS. \quad (19)$$

where  $S$  represents the total length of the upper wavy surface.

The friction factor of the wavy channel is:

$$f = \frac{2D_h \Delta P}{L \rho_f u_m^2}. \quad (20)$$

where  $D_h$  is the wavy channel hydraulic diameter and  $u_m$  is the mean velocity.

## Numerical method and validations

Using the Galerkin weighted residual finite element technique, the dimensionless pattern of the governing Eqs. (8)–(13) managed by the implemented dimensionless boundary conditions (14)–(17) continues proposed. The computational area is decomposed into triangular elements as revealed in Fig. 2. For each of the flow and temperature ranges within the computational area, triangular Lagrange finite elements of various orders are used.

Substitution of approximations inside the governing equations yields the residuals of all conservation equations. A Newton-Raphson iteration algorithm is used to explain the nonlinear expressions within the momentum equations; additionally, the convergence regarding the solution remains appropriate although the corresponding error of the variables fulfills the resulting convergence criterion:

$$\left| \frac{\Gamma^{i+1} - \Gamma^i}{\Gamma^{i+1}} \right| \leq \eta.$$

For assuring the independence of the existing numerical solution toward the grid size of the numerical domain, different grid sizes are applied to calculate the average Nusselt number ( $\bar{Nu}$ ), the minimum strength of the flow circulation ( $\Psi_{min}$ ) and the minimum strength of the heatfunction ( $H_{min}$ ) for the case of  $Re = 40,000, N = 4, A = 0.1$  and  $Pr = 4.623$ . The results are exhibited in Table 1 and show insignificant variations toward the G5 grid and beyond. Hence, for all computations of this study, the G5 uniform grid is applied.

Furthermore, toward the idea of confirming the current numerical data, the resulting outcomes are associated with the experimental outcomes described by Chen and Wang [34] for the problem of forced convection turbulent flow and heat transfer within a 2D horizontal channel, as revealed in

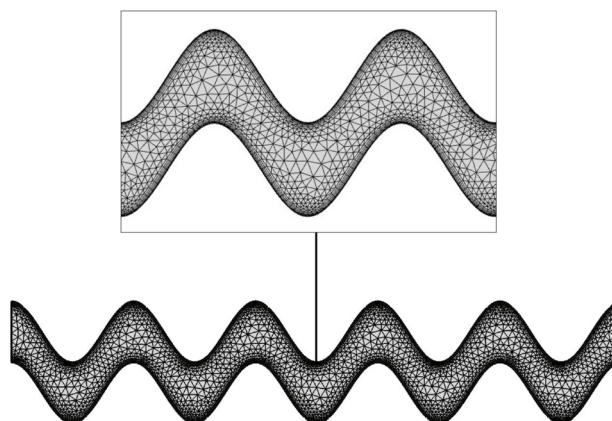


Fig. 2 FEM grid-points distribution for the grid size of 3748 elements.

**Table 1** Grid testing for the average Nusselt number  $\overline{Nu}$  and the average skin friction factor (ASFC) at different grid sizes for  $Re = 40,000$ ,  $N = 4$  and  $A = 0.1$ .

Grid size	Number of elements	$\overline{Nu}$	ASFC
G1	3748	79.486	0.19179
G2	4863	80.606	0.19578
G3	7141	82.394	0.19806
G4	9449	84.199	0.21238
<b>G5</b>	24768	84.211	0.21404
G6	69772	84.216	0.21415

Fig. 3. Moreover, we compared the average Nusselt number of the experimental outcomes of Kilicaslan and Sarac [35] and Elshafei et al. [36] and the friction factor with the experimental outcomes of Promvonge and Thianpong [37] and Eiamsa-Ard and Promvonge [38] concerning various

values of Reynolds number, as designated in Fig. 4a and b. Such outcomes appear through those validations produce significant confidence in the efficiency of the existing numerical scheme.

### Results and discussion

Within this section, we shall present the streamlines, isotherms, turbulent kinetic energy, local and average skin friction coefficient including Nusselt number. The dimensionless parameters are Reynolds number ( $10^3 \leq Re \leq 10^5$ ), number of oscillations ( $0 \leq N \leq 5$ ), amplitude ( $0.05 \leq A \leq 0.2$ ) and the value of the Prandtl number remains fixed at  $Pr = 4.623$ .

The streamlines, isotherms and the turbulent kinetic energy isolines are displayed in Fig. 5 for various values of the Reynolds number. It is well known that a rise of this

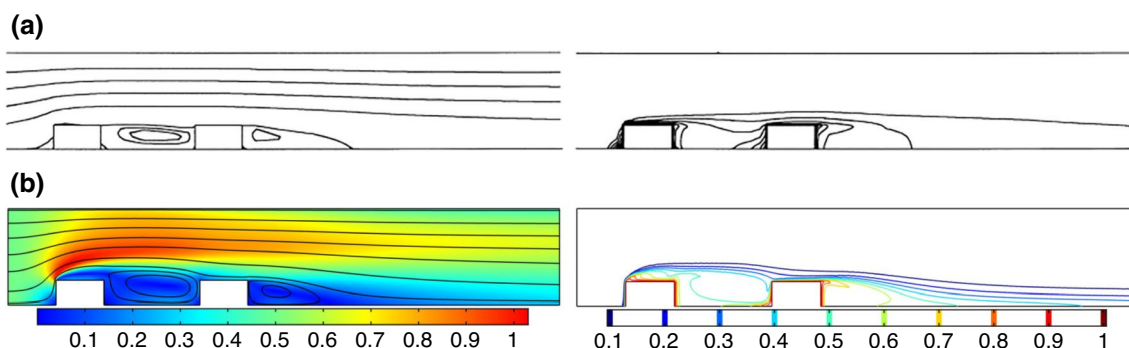


Fig. 3 a Chen and Wang [34] and b present study; (left) velocity (streamlines) and (right) isotherms at  $Re = 10000$ ,  $N = 0$  and  $A = 0$ .

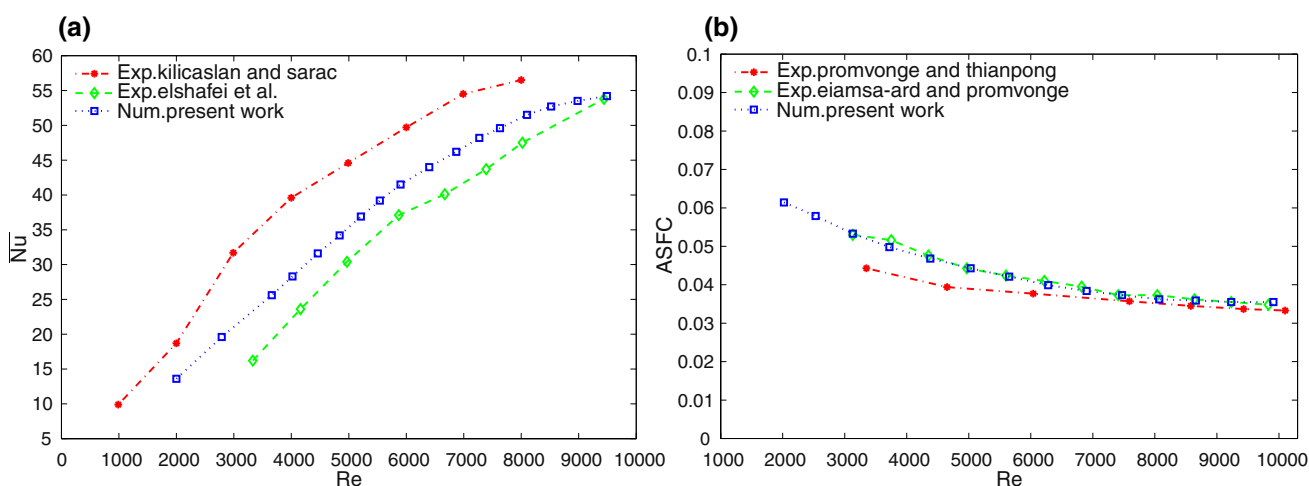


Fig. 4 Comparison of a average Nusselt number with Reynolds number from the present numerical code with the experimental results of Kilicaslan and Sarac [35] and Elshafei et al. [36] and b average skin friction factor with Reynolds number from the present

numerical code with the experimental results of Promvonge and Thianpong [37] and Eiamsa-Ard and Promvonge [38] for different values of Rayleigh numbers.

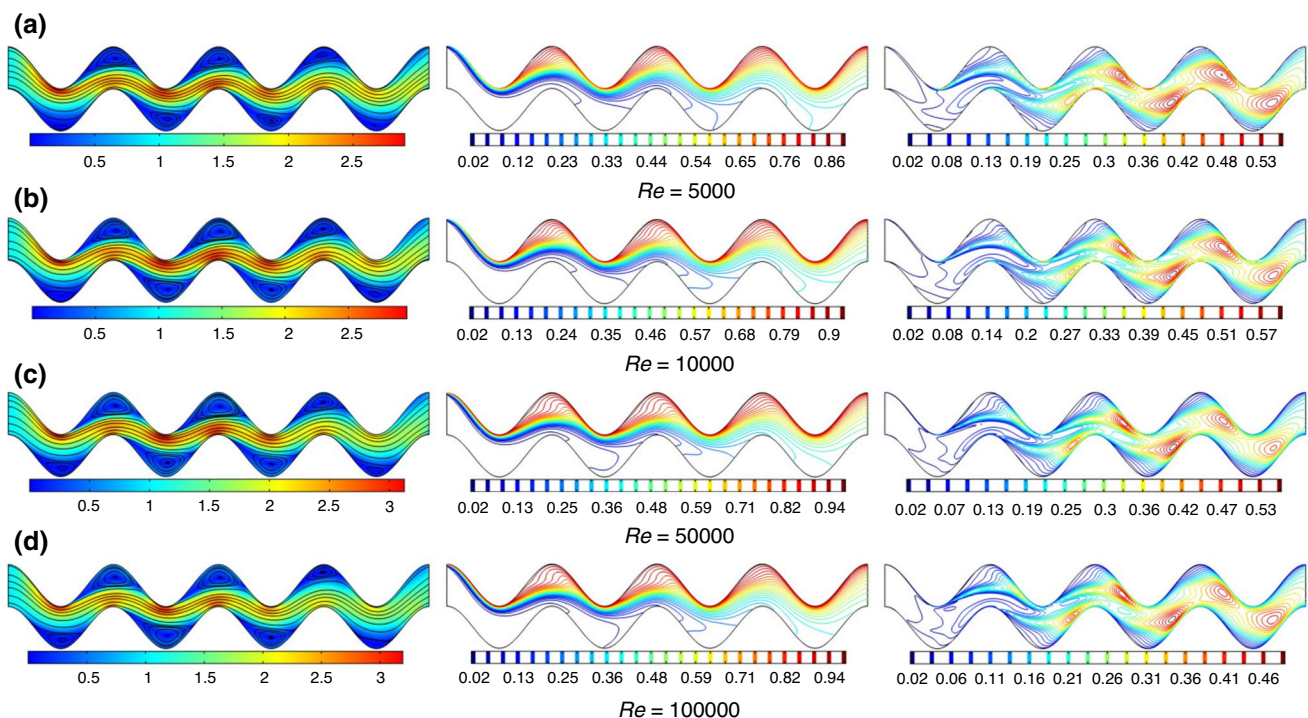
dimensionless parameter characterizes a growth of flow strength. As a result, the flow velocity increases and the recirculations zones become greater. The latter describes the flow straightening, and therefore recirculation zones within the wave troughs are enhanced. About an identical time, the temperature field reveals cooling of the channel from the inlet and heating from the upper wall. It seems that the growth of  $Re$  does not have any substantial influence due to an essential resistance regarding the shape of the channel. Regardless of the Reynolds number, cooling from the inlet allows to remove the heating effect significantly from the first trough, but next troughs are heated strongly. The distribution of turbulent kinetic energy characterizes essential production of it from the channel borders near the wave picks in the second half of the channel.

Figure 6 exposes the change of the local Nusselt number and skin friction factor along the heated upper surface toward various rates of Reynolds number. The wave behaviour of these parameters is due to the wave nature of the wall. As for the local Nusselt number, it is possible to highlight here that maximum values of  $Nu$  correspond to wave picks due to the high-temperature gradient and low thickness of the thermal boundary layer. In contrast, minimum values correspond to the wave troughs where recirculations are formed, and the temperature gradient is low. Rise of the above wavy surface coordinate reflects a reduction of the maximum values of the local Nusselt number affected

with the limited intensive cooling of the surface. Toward an equivalent time, a growth of the Reynolds number portrays an increase of the local Nusselt number. Simultaneously, the skin friction factor has similar behaviour, where the location of maximum and minimum values is identical to the conduct of the local Nusselt number. It makes worthy specifying that a rise of  $Re$  depicts a decline of the skin friction factor, while the local heat transfer improves. Such a situation is desirable for any engineering apparatus.

An influence of the waviness number on streamlines, isotherms and turbulent kinetic energy field for  $Re = 40,000$  and  $A = 0.1$  is demonstrated in Fig. 7. A growth of  $N$  leads to an appearance of recirculations within the wave troughs with a reduction of the temperature gradient in these zones. At the same time, a presence of waviness allows to accelerate the flow within the channel, while the thermal boundary layer thickness increases with waviness. An appearance of recirculations within the wave troughs characterizes a formation of more stable central part of flat flow that leads to an acceleration of flow. Fields of the turbulent kinetic energy illustrate a generation of this energy near the channel walls, while a rise of the waviness number illustrates an appearance of kinetic energy generation zones near the wave picks.

An influence of the undulations number on the local Nusselt number and skin friction factor is presented in Fig. 8. A rise of  $N$  characterizes a formation of wavy behavior of these considered parameters. Oscillation



**Fig. 5** Variations of (left) velocity (streamlines), (middle) isotherms, and (right) turbulent kinetic energy; evolution by Reynolds number ( $Re$ ) for  $N = 4$  and  $A = 0.1$ .

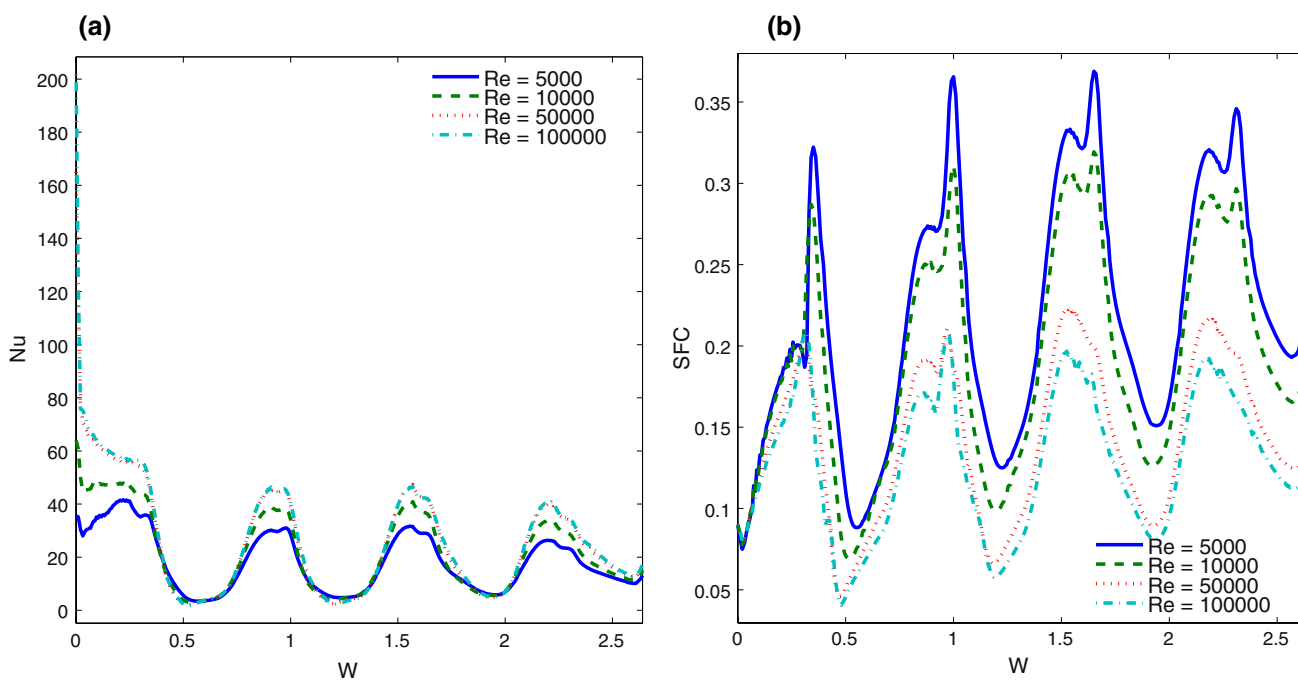


Fig. 6 Variations of **a** local Nusselt numbers interface with  $S$  and **b** skin friction factor for different  $Re$  at  $N = 4$  and  $A = 0.1$ .

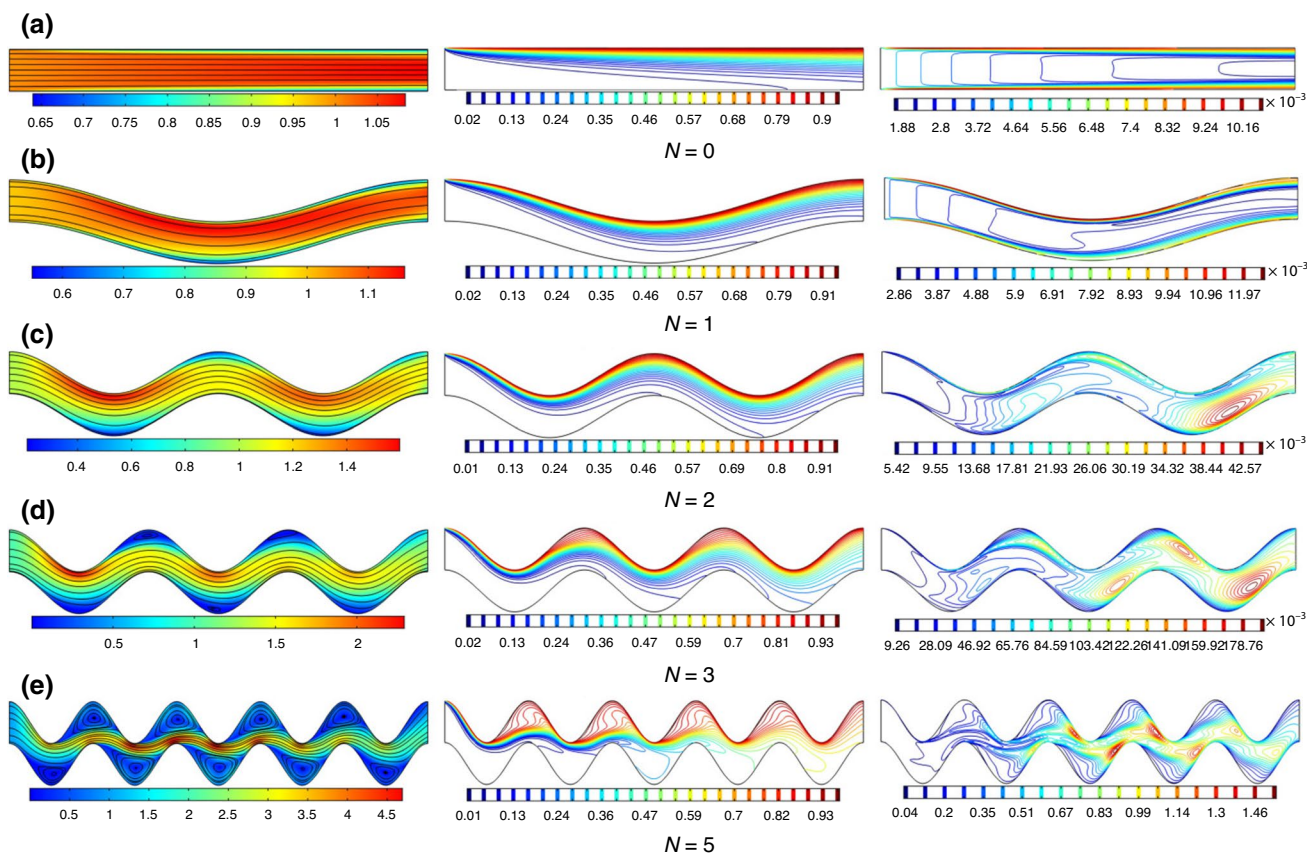
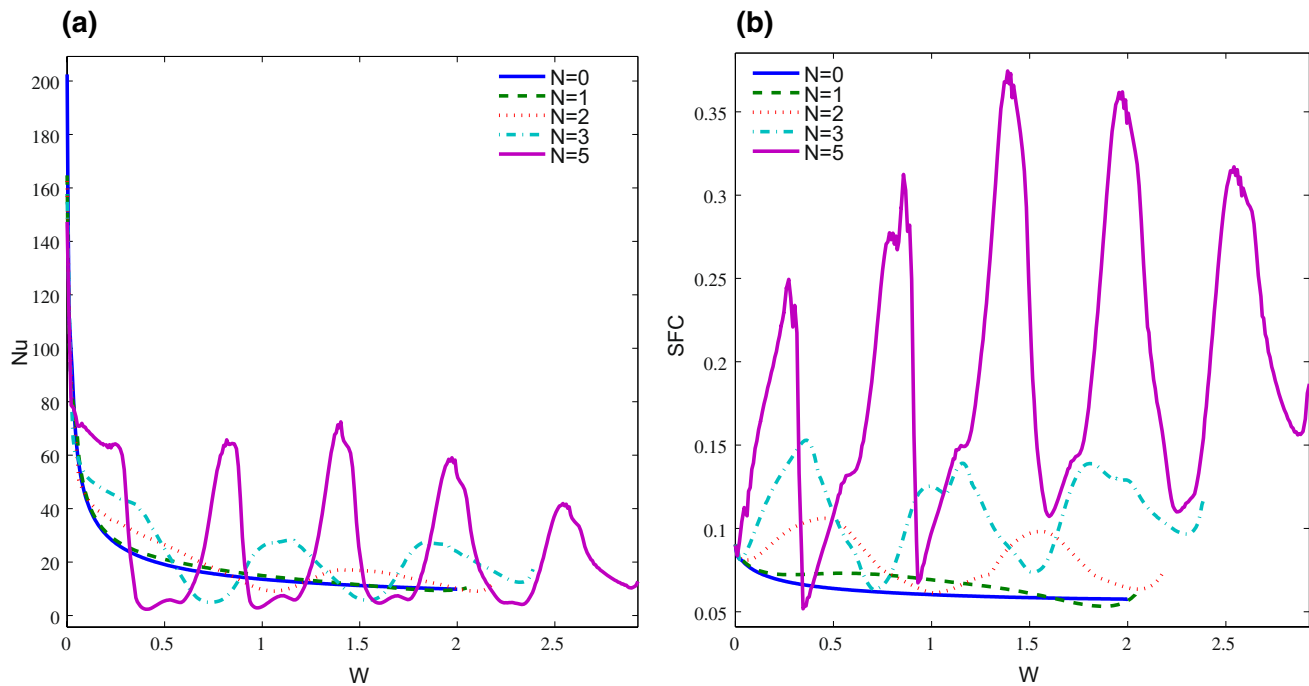


Fig. 7 Variations of (left) velocity (streamlines), (middle) isotherms, and (right) turbulent kinetic energy; evolution by number of oscillations ( $N$ ) for  $Re = 40,000$  and  $A = 0.1$ .



**Fig. 8** Variations of **a** local Nusselt numbers interface with  $S$  and **b** skin friction factor for different  $N$  at  $Re = 40,000$  and  $A = 0.1$ .

amplitude of  $Nu$  and skin friction factor increases with  $N$ . It should be noted that minimum values correspond to the flat channel, while the maximum values increase with waviness number. A reduction of the local Nusselt number with the length of the upper wall is due to an attenuation of the cooling effect from the inlet under the heating of the upper wavy wall.

Figure 9 reflects an effect of the wavy walls amplitude on isolines of stream function, temperature and turbulent kinetic energy. For high amplitude of the channel walls the flow should surround each wave crest and as a result the skin friction factor increases essentially (see Fig. 10) and the cooling effect becomes weak for wave troughs located near the outlet. The turbulent kinetic energy field illustrates a formation of generation zones near the wave crests and these zones move toward to the inlet with a rise of  $A$ . Local Nusselt number and skin friction factor are increased in amplitude of the oscillations with wavy wall amplitude.

Moreover, a formation of extended heat transfer surface allows to extend the heat removal effect.

The role regarding the average Nusselt number and average skin friction factor with the governing parameters is presented in Figs. 11 and 12. It should be noted that these parameters repeat the performance of the local characteristics, where behavior of local Nusselt number and skin friction parameter is similar to the case of an influence of the wall waviness (see Fig. 8). Therefore, the average Nusselt number, and as an outcome, the heat transfer rate denotes a rising function of the Reynolds number, undulations number and wavy wall amplitude. At the same time, the average skin friction factor decreases with  $Re$  but increases with  $N$  and  $A$ . It should be noted that more essential raise of the average Nusselt number with undulations number occur for high values of the Reynolds number, while in the case of average skin friction parameter one can find such effect for low Reynolds number. In conclusion, it remains possible for determining the optimal values of these governing parameters for essential heat removal and not so strong flow resistance.

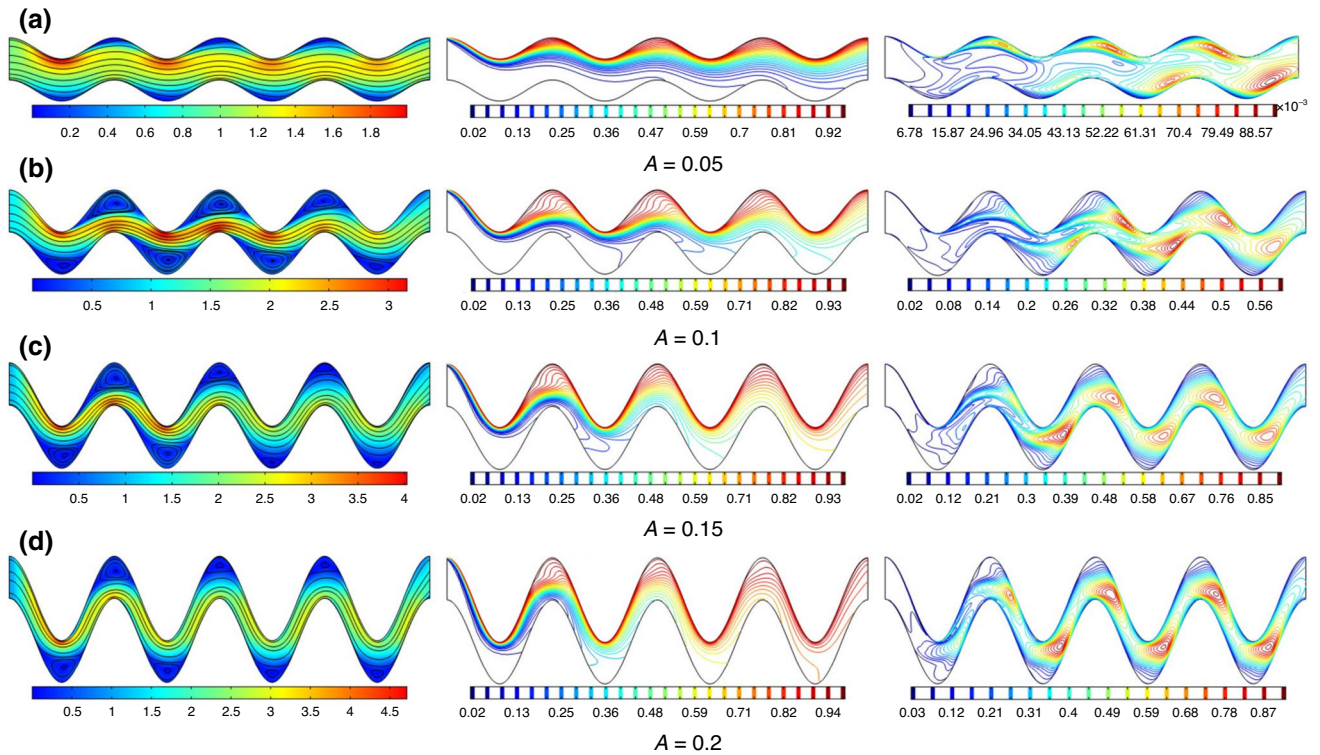


**Fig. 9** Variations of (left) velocity (streamlines), (middle) isotherms, and (right) turbulent kinetic energy; evolution by amplitude ( $A$ ) for  $Re = 40,000$  and  $N = 4$ .

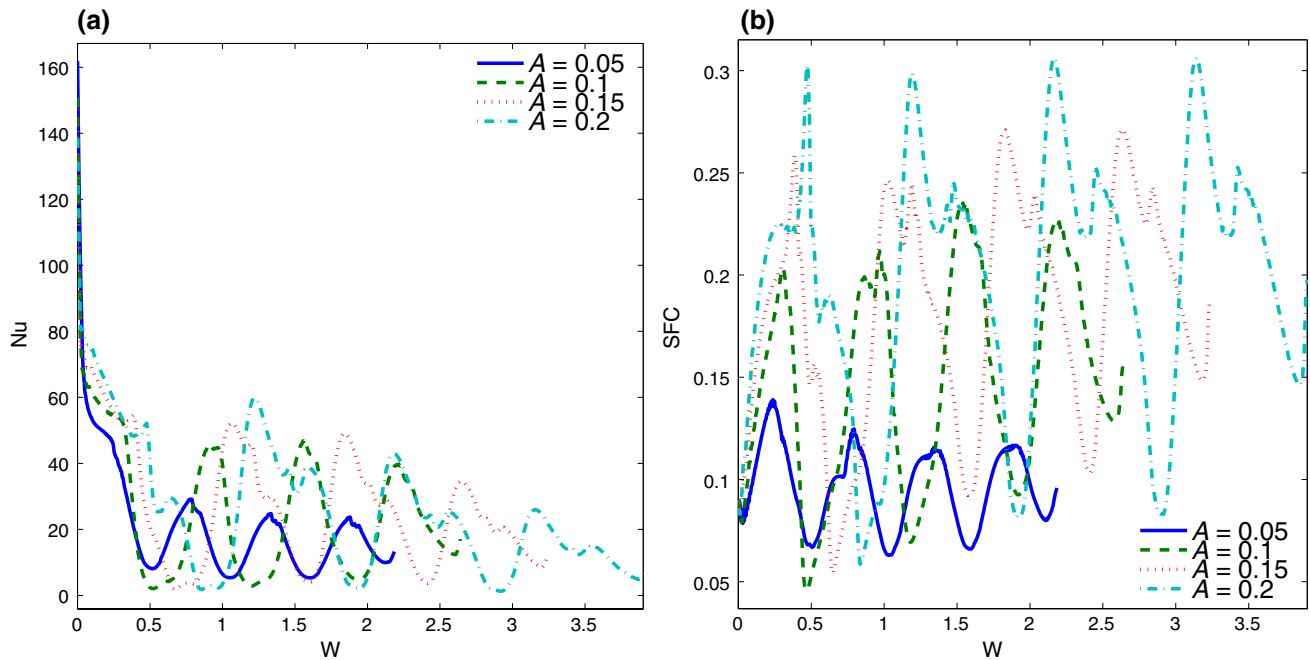


**Fig. 10** Variations of **a** local Nusselt numbers interface with  $S$  and **b** skin friction factor for different  $A$  at  $Re = 40,000$  and  $N = 4$ .

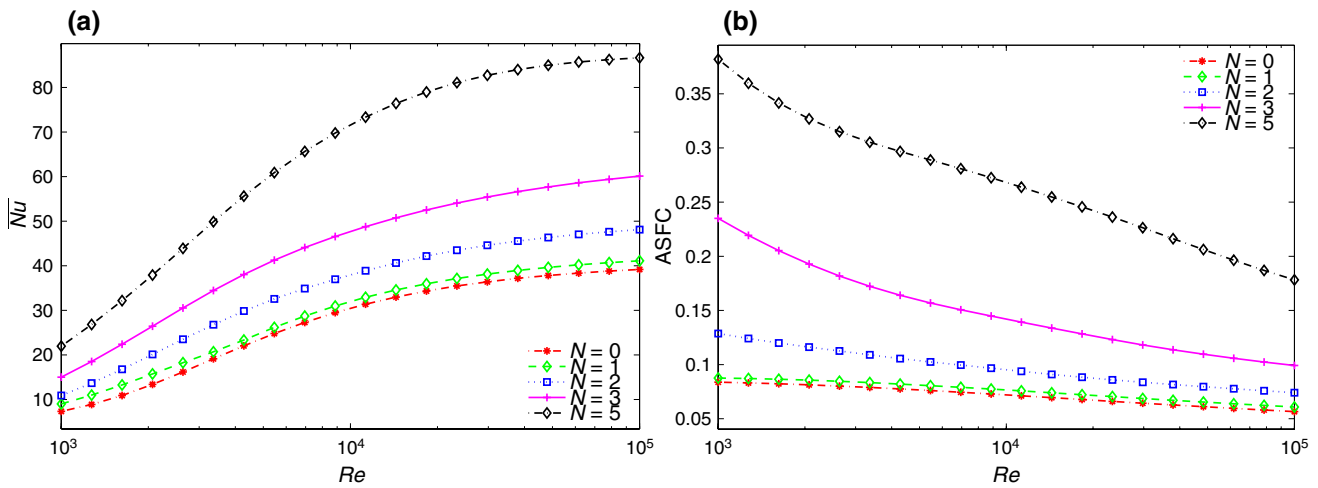


Fig. 11 Variations of **a** average Nusselt number and **b** average skin friction factor with  $Re$  for different  $N$  at  $A = 0.1$ .

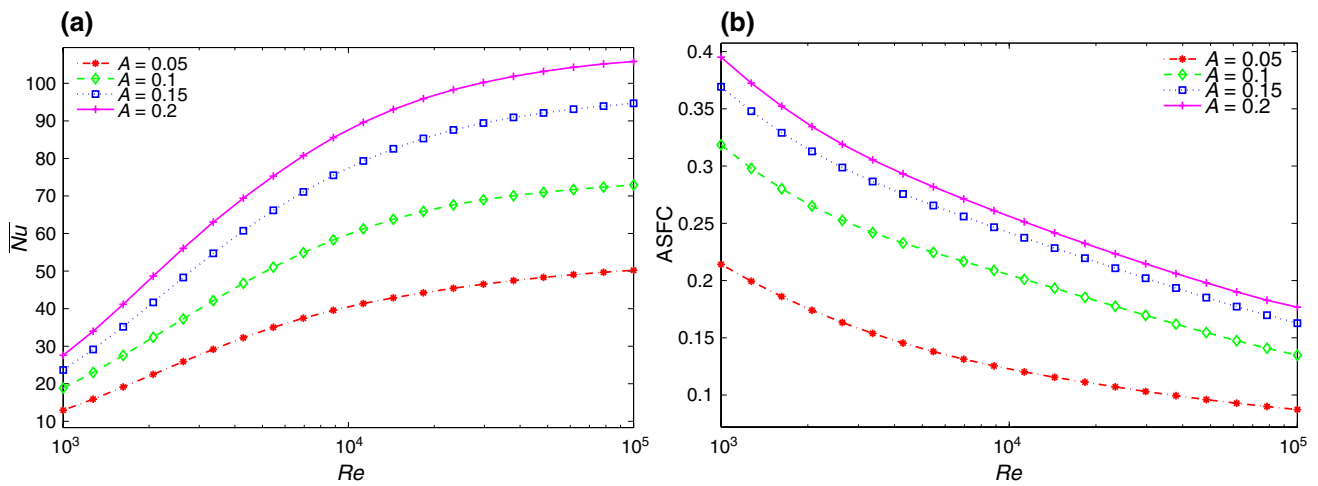


Fig. 12 Variations of **a** average Nusselt number and **b** average skin friction factor with  $Re$  for different  $A$  at  $N = 4$ .

## Conclusions

The turbulent forced convection within a wavy channel having an isothermal upper wavy wall has been numerically examined by adopting the finite element procedure. Influences of the Reynolds number, undulations number, and wavy walls amplitude toward fluid flow and heat transfer have been considered. Throughout the investigation, the following outcomes have been observed.

1. A rise of the Reynolds number indicates an acceleration of the flow with an increase of the energy transport strength and a decline in flow resistance.
2. A growth of the undulations number characterizes the recirculation zones' appearance and an extension of the heat transport intensity and skin friction factor through

an identical time. In comparison, an increase regarding the wavy surface amplitude points to the addition of the recirculation area. As a result, defining these governing parameters optimal rates for essential heat removal and not so strong flow resistance remains possible. Moreover, an addition of waviness in a channel generates oscillating behavior of the local Nusselt number, where maximum values can be greater of the flat channel case up to 4 times. While the average Nusselt number rises up to 2 times between the flat channel and wavy channel with 5 undulations. Such influence becomes stronger for high values of the Reynolds number. Average skin friction factor increases with channel waviness, but more essential raise can be found for low values of the Reynolds number. It is interesting to note that for  $Re = 10^3$  an increase of  $N$  from 0 till 5 leads to a growth of ASFC

up to 4 times, while for  $Re = 10^5$  an increase of  $N$  from 0 till 5 leads to a growth of ASFC up to 3 times.

3. A rise of the wavy channel amplitude increases the average Nusselt number and average skin friction factor. In the case of heat transfer an effect is more essential for high Reynolds numbers, whilst for flow resistance it is more visible for low Reynolds numbers.

The obtained results characterize an opportunity to augment the heat transfer and reduce the flow resistance for a high Reynolds number, high undulations number and wavy walls amplitude. It should be noted that from a practical point of view, the future research can be related to an analysis of an influence of pulsating flow and boundary heat flux.

**Acknowledgements** The work was supported by the Universiti Kebangsaan Malaysia (UKM) research grant GP-2021-K006388. This research of M.A. Sheremet was supported by the Tomsk State University Development Programme (Priority-2030). We thank the respected reviewers for their constructive comments which clearly enhanced the quality of the manuscript.

## References

1. Kumar A, Kim MH. Convective heat transfer enhancement in solar air channels. *Appl Therm Eng.* 2015;89:239.
2. Shenoy A, Sheremet M, Pop I. Convective flow and heat transfer from wavy surfaces: viscous fluids, porous media, and nanofluids. Boca Raton: CRC Press; 2016.
3. Wilk J. Heat/mass transfer analogy in the case of convective fluid flow through minichannels. *Int J Therm Sci.* 2020;156: 106467.
4. Zheng N, Yan F, Zhang K, Zhou T, Sun Z. A review on single-phase convective heat transfer enhancement based on multi-longitudinal vortices in heat exchanger tubes. *Appl Therm Eng.* 2020;164: 114475.
5. Sheikholeslami M, Jafaryar M. Nanoparticles for improving the efficiency of heat recovery unit involving entropy generation analysis. *J Taiwan Inst Chem Eng.* 2020;115:96.
6. Nagarani N, Mayilsamy K, Murugesan A, Kumar GS. Review of utilization of extended surfaces in heat transfer problems. *Renew Sustain Energy Rev.* 2014;29:604.
7. Pandya NS, Shah H, Molana M, Tiwari AK. Heat transfer enhancement with nanofluids in plate heat exchangers: a comprehensive review. *Eur J Mech B.* 2020;81:173.
8. Miroshnichenko IV, Sheremet MA, Pop I, Ishak A. Convective heat transfer of micropolar fluid in a horizontal wavy channel under the local heating. *Int J Mech Sci.* 2017;128:541.
9. Vo DD, Alsarraf J, Moradikazerouni A, Afrand M, Salehipour H, Qi C. Numerical investigation of  $\gamma$ -AlOOH nano-fluid convection performance in a wavy channel considering various shapes of nanoadditives. *Powder Technol.* 2019;345:649.
10. Dormohammadi R, Farzaneh-Gord M, Ebrahimi-Moghadam A, Ahmadi MH. Heat transfer and entropy generation of the nanofluid flow inside sinusoidal wavy channels. *J Mol Liq.* 2018;269:229.
11. Jamshidmofid M, Bahiraei M. Hydrothermal performance of single and hybrid nanofluids in left-right and up-down wavy micro-channels using two-phase mixture approach. *Int Commun Heat Mass Transf.* 2021;129: 105752.
12. Alrowaili D, Ahmed SE, Elshehabeey HM, Ezzeldien M. Magnetic radiative buoyancy-driven convection of MWCNTs- $C_2H_6O_2$  power-law nanofluids in inclined enclosures with wavy walls. *Alex Eng J.* 2022;61(11):8677.
13. Kumar R, Tiwary B, Singh PK. Thermofluidic analysis of  $Al_2O_3$ -water nanofluid cooled branched wavy heat sink. *Appl Therm Eng.* 2022;201: 117787.
14. Jahanbakhshi A, Nadooshan AA, Bayareh M. Cooling of a lithium-ion battery using microchannel heatsink with wavy micro-tubes in the presence of nanofluid. *J Energy Storage.* 2022;49: 104128.
15. Mohammed HA, Vuthaluru HB, Liu S. Thermohydraulic and thermodynamics performance of hybrid nanofluids based parabolic trough solar collector equipped with wavy promoters. *Renew Energy.* 2022;182:401.
16. Derikvand M, Rahmati AR. Numerical investigation of power-law hybrid nanofluid in a wavy micro-tube with the hydrophobic wall and porous disks under a magnetic field. *Int Commun Heat Mass Transf.* 2021;129: 105633.
17. Perng SW, Wu HW. Effect of sinusoidal-wavy channel of reformer on power of proton exchange membrane fuel cell. *Appl Therm Eng.* 2019;162: 114269.
18. Borgohain P, Choudhary D, Dalal A, Natarajan G. Numerical investigation of mixing enhancement for multi-species flows in wavy channels. *Chem Eng Process-Process Intensif.* 2018;127:191.
19. Nguyen TK, Saidizad A, Jafaryar M, Sheikholeslami M, Gerdroodbary MB, Moradi R, Shafee A, Li Z. Influence of various shapes of CuO nanomaterial on nanofluid forced convection within a sinusoidal channel with obstacles. *Chem Eng Res Des.* 2019;146:478.
20. Khoshvaght-Aliabadi M, Hassani SM, Mazloumi SH. Enhancement of laminar forced convection cooling in wavy heat sink with rectangular ribs and  $Al_2O_3$ /water nanofluids. *Exp Therm Fluid Sci.* 2017;89:199.
21. Yuan D, Zhou W, Fu T, Liu C. Experimental and numerical investigation of heat and mass transfer in non-uniform wavy microchannels. *Int J Therm Sci.* 2020;152: 106320.
22. Job VM, Gunakala SR. Mixed convection nanofluid flows through a grooved channel with internal heat generating solid cylinders in the presence of an applied magnetic field. *Int J Heat Mass Transf.* 2017;107:133.
23. Job VM, Gunakala SR. Mixed convective ferrofluid flow through a corrugated channel with wall-mounted porous blocks under an alternating magnetic field. *Int J Mech Sci.* 2018;144:357.
24. Yang YT, Wang YH, Tseng PK. Numerical optimization of heat transfer enhancement in a wavy channel using nanofluids. *Int Commun Heat Mass Transf.* 2014;51:9.
25. Manglik RM, Zhang J, Muley A. Low Reynolds number forced convection in three-dimensional wavy-plate-fin compact channels: fin density effects. *Int J Heat Mass Transf.* 2005;48(8):1439.
26. Sui Y, Teo CJ, Lee PS. Direct numerical simulation of fluid flow and heat transfer in periodic wavy channels with rectangular cross-sections. *Int J Heat Mass Transf.* 2012;55(1-3):73.
27. Forooghi P, Hooman K. Effect of buoyancy on turbulent convection heat transfer in corrugated channels—a numerical study. *Int J Heat Mass Transf.* 2013;64:850.
28. Ramgadia AG, Saha AK. Study of fully-developed turbulent flow and heat transfer in a rotating wavy-walled duct. *Int J Heat Mass Transf.* 2019;144: 118578.
29. Ahmadpour A, Abadi SMANR. Thermal-hydraulic performance evaluation of gas-liquid multiphase flows in a vertical sinusoidal wavy channel in the presence/absence of phase change. *Int J Heat Mass Transf.* 2019;138:677.

30. Ajeel RK, Salim WI, Sopian K, Yusoff MZ, Hasnan K, Ibrahim A, Al-Waeli AHA. Turbulent convective heat transfer of silica oxide nanofluid through corrugated channels: an experimental and numerical study. *Int J Heat Mass Transf.* 2019;145: 118806.
31. Ajeel RK, Salim WI, Hasnan K. Experimental and numerical investigations of convection heat transfer in corrugated channels using alumina nanofluid under a turbulent flow regime. *Chem Eng Res Des.* 2019;148:202.
32. Al-Zurfi N, Alhusseney A, Nasser A. Effect of rotation on forced convection in wavy wall channels. *Int J Heat Mass Transf.* 2020;149: 119177.
33. Sheikholeslami M, Jafaryar M, Said Z, Alsabery AI, Babazadeh H, Shafee A. Modification for helical turbulator to augment heat transfer behavior of nanomaterial via numerical approach. *Appl Therm Eng.* 2021;182: 115935.
34. Chen YM, Wang KC. Experimental study on the forced convective flow in a channel with heated blocks in tandem. *Exp Therm Fluid Sci.* 1998;16(4):286.
35. Kilicaslan I, Sarac HI. Enhancement of heat transfer in compact heat exchanger by different type of rib with holographic interferometry. *Exp Therm Fluid Sci.* 1998;17(4):339.
36. Elshafei EAM, Awad MM, El-Negiry E, Ali AG. Heat transfer and pressure drop in corrugated channels. *Energy.* 2010;35(1):101.
37. Promvong P, Thianpong C. Thermal performance assessment of turbulent channel flows over different shaped ribs. *Int Commun Heat Mass Transf.* 2008;35(10):1327.
38. Eiamsa-Ard S, Promvong P. Thermal characteristics of turbulent rib-grooved channel flows. *Int Commun Heat Mass Transf.* 2009;36(7):705.

**Publisher's Note** Springer Nature remains neutral with regard to jurisdictional claims in published maps and institutional affiliations.